Proceedings of the Sixth International Conference on
Railway Technology: Research, Development and Maintenance
Edited by: J. Pombo
Civil-Comp Conferences, Volume 7, Paper 22.3
Civil-Comp Press, Edinburgh, United Kingdom, 2024
ISSN: 2753-3239, doi: 10.4203/ccc.7.22.3
©Civil-Comp Ltd, Edinburgh, UK, 2024

A PDEM-Based Research on the Impact of Stochasticity in the Inside Distance Between the Wheelset on the Vehicle-Turnout Coupling System

Z. Yan[1,2], T. Li[1,2], J. Chen[1,2], J. Xu[1,2], P. Wang[3,2] and R. Chen[1,2]

[1]Key Laboratory of High-Speed Railway Engineering, Ministry of Education, Southwest Jiaotong University, Chengdu, China
[2]School of Civil Engineering, Southwest Jiaotong University, Chengdu, China
[3]Key Laboratory of High-Speed Railway Engineering, Ministry of Education, Southwest Jiaotong University, Chengdu, China

Abstract

The inside distance between the wheelset is one of the most important influencing factors of the wheel-rail contact. By varying this factor, the corresponding comprehensive performance of a train passing through a turnout is hard to demonstrate through traditional methods. The application of stochastic theory is crucial. This paper constructs a stochastic field of variation of the inside distance between the wheelset. By employing the modal superposition method, a coupled vehicle-turnout multi-body dynamics system was built with rail flexibility considered via the ABAQUS-SIMPACK platform. The probability density function (PDF) of lateral displacement of the wheelset and the vertical wheel force were determined based on the generalized probability density equation (GDEE). The results show that the variation of inside distance between the wheelset can cause dispersion of lateral displacement of the wheelset in both the closure panel and the area behind the wheel load transition in the crossing panel. The vertical wheel forces in both the switch panel and the crossing panel present a more significant stochasticity while relatively concentrated in other areas. The maximum variation range is approximately 5 kilonewton (kN). Increase of the inside distance between the wheelset can exacerbate the lateral deviation of the wheelset towards the straight stock rail during wheel load transition in the switch panel, and can make the wheelset easier to align with the centreline of the track. The position of wheel load transition is advanced from about 240 to 250 mm in the switch panel, while that in the crossing panel hardly changes.

Keywords: inside distance between the wheelset, lateral displacement of wheelset, vertical wheel force, generalized density evolution equation, probability density function, wheel load transition.

1 Introduction

The core of achieving a smooth, safe and reliable train journey is the good wheel-rail contact. The wheel-rail matching performance is directly affected by multiple wheel-rail contact geometry parameters, such as wheel tread, rail head profile, gauge, etc. The inside distance between the wheelset describes the perpendicular distance between two wheel flanges of the same wheelset. Deviation of this index changes the clearance between the wheel flange and the rail gauge corner, potentially leading to hunting motion and instability of the train. Many researchers have conducted a large number of relevant studies on this issue and significant results and progress have been achieved. Based on the railway roller rig, H. C. Chen, et al. [1, 2] found that increasing the inside distance between the wheelset will increase the equivalent taper of wheel-rail contact and reduces the critical speed of train running. The geometric relationship between this index and the gap in the fixed crossing panel in scenarios of three types of wheel tread were also analysed. G. W. Xiao, et al. [3], R. Chen, et al. [4], N, Wu, et al. [5], C, G, Wang, et al. [6] have all compared the static wheel-rail contact geometry in a track or a turnout under different wheel treads and different inside distances between the wheelset. Recommendations for optimal match of wheel tread and inside distance between the wheelset have been offered. The research of R, Luo, et al. [7] indicates that increasing the inside distance between the wheelset of the wheelset with LMA tread will aggravate its wheel wear and drive the wear extending towards the flange. Similarly, Y, Y, Qi, et al. [8] found that reducing the distance between wheel flanges can not only decreases the equivalent conicity but also significantly reduces the lateral acceleration of the car-body and the frame. H, L, Shi, et al. [9] analysed the compatibility between rail cant, wheel tread and inside distance between the wheelset. The amplitude-frequency characteristics of the dynamic variation of inside distance between the wheelset was obtained. Q, S, Zhang, et al. [10] have designed an online measurement system for wheelset geometry determination based on a two-dimensional laser-displacement sensor. This system can reduce the error to less than 0.5 mm in the measurement of inside distance between the wheelset. The accuracy and efficiency were thus improved.

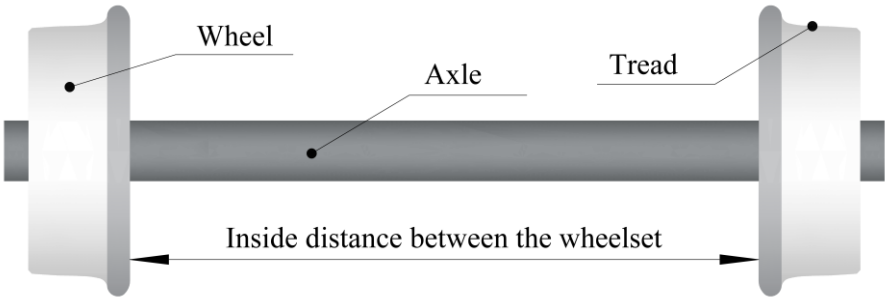

Figure 1: The inside distance between the wheelset.

The vast majority of existing researches, including the multi-body dynamics simulation, the static contact mechanics and the finite element model, are based on the assumption of parameter certainty. The wheel-rail geometry, including the inside distance between the wheelset, is considered to be fixed, yielding the most ideal condition. In fact, the inside distance between the wheelset is not certain due to the manufacturing error and axle bending [11]. In addition, there is a lack of comprehensive statistics of distribution of dynamic performance of the train passing through a turnout under different inside distances between the wheelset. On the other hand, the turnout, as the only remaining weakness in high-speed railway nowadays, serves as a key equipment for guiding the train change or crossover a track in the vast railway network. The turnout consists of numerous track components, resulting in structural irregularities. The wheel-rail contact in a turnout is more complex compared to that in a straight or curved track, posing an only threat to the stability, safety and comfort of the train running in the entire railway section. However, the relevant studies on the impact of inside distance between the wheel set on the dynamic performance of the train passing through a turnout is still insufficient. The corresponding stochastic characteristics of related wheel load transition has not been fully understood.

Given above issues, it is necessary to illustrate the impact of uncertainty of inside distance between the wheelset on vehicle dynamic performance from the perspective of probability theory. For random parameters in the coupled vehicle-turnout dynamics system, some mature stochastic theoretical methods, such as the second-order perturbation theory [12], the orthogonal polynomial expansion [13], the Monte Carlo sampling [14], et al, can be employed. The probability density evolution method (PDEM), proposed by J, Li and J, B, Chen [14] and based on the principle of probability conservation, has overcome the difficulty of traditional methods in dealing with random dynamic responses of nonlinear systems, and significantly improves the accuracy and efficiency of system response analysis and reliability calculations. Therefore, this paper has constructed a stochastic field of the inside distance between the wheelset to study the corresponding impact on the dynamic performance of the train passing through a turnout. The coupled vehicle-turnout model was built via the multi-body dynamics simulation platform SIMPACK. The rail flexibility was considered within the finite element platform ABAQUS. By utilizing the GDEE, the PDF of dynamic wheel-rail interactions were described and analysed. This research reveals the mechanism of wheel load transition under different inside distances between the wheelset and corresponding stochastic distribution of the dynamic wheel-rail interactions.

2 Model

2.1 The vehicle model

To build the simulation model of a high-speed powered vehicle, the CRH 380A EMU train, commonly used in China’s high-speed railway, were taken as a prototype. The model comprises major components such as the car-body, the frame, the axle guide,

and the wheelset. Each component is considered as a rigid body and assigned with corresponding mass and moment of inertia, as shown in Table 1. Apart from the hinge unit of the axle guide that is used to connect the axle guide and the wheelset, most massless hinge units serve as the connection between the car-body component and the ground system, with certain degrees of freedom to reflect the corresponding movement. The car-body, the frame and the wheelset each have six degrees of freedom, including heave, sway, surge, yaw, roll and pitch. The axle guide, on the other hand, only has one degree of freedom, i.e., pitch. The connections between various components are achieved via the spring-damping units. Specifically, the car-body and the frame are connected via the secondary suspension system, which includes secondary coil springs, secondary vertical shock absorbers, anti-torsion rods, anti-hunting vibration absorbers, lateral stops, etc. The frame and the axle guide that is located on the end of the axle are connected by the primary suspension system, which includes primary coil springs, primary vertical shock absorbers, etc. The stiffness and damping characteristics of the main force transmission unit are listed in Table 2.

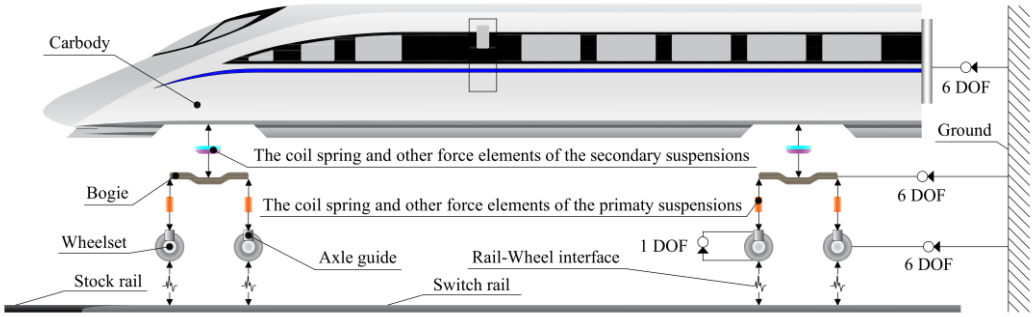

Figure 2: The simplified topology of the vehicle model.

Major parameters	Value	Unit
Mass of the carbody (empty)	34934	kg
Moment of inertia of the carbody around the x axis	113200	$kg \cdot m^2$
Moment of inertia of the carbody around the y axis	1711800	$kg \cdot m^2$
Moment of inertia of the carbody around the z axis	1615300	$kg \cdot m^2$
Mass of the bogie	3300	kg
Moment of inertia of the bogie around the x axis	2673	$kg \cdot m^2$
Moment of inertia of the bogie around the y axis	1807	$kg \cdot m^2$
Moment of inertia of the bogie around the z axis	3300	$kg \cdot m^2$
Mass of the axle guide	48.2	kg
Moment of inertia of the axle guide around the x axis	0.72	$kg \cdot m^2$
Moment of inertia of the axle guide around the y axis	2.76	$kg \cdot m^2$
Moment of inertia of the axle guide around the z axis	2.62	$kg \cdot m^2$
Mass of the wheelset	1780	kg
Moment of inertia of the wheelset around the x axis	949	$kg \cdot m^2$
Moment of inertia of the wheelset around the y axis	118	$kg \cdot m^2$
Moment of inertia of the wheelset around the z axis	967	$kg \cdot m^2$

Table 1. Major mass and inertial parameters of the vehicle model.

Major parameters	Value	Unit
Lateral stiffness of the primary suspension	980	kN/m
Vertical stiffness of the primary suspension	1176	kN/m
Vertical damping of the primary suspension	10	kN·s/m
Lateral stiffness of the secondary suspension	160	kN/m
Vertical stiffness of the secondary suspension	240	kN/m
Vertical damping of the secondary suspension	20	kN·s/m

Table 2. Major suspension system parameters of the vehicle model.

The wheel-rail contact interface is the key to achieving the mutual coupling between the isolated vehicle and turnout system. The spline curves were employed to smoothen the discrete data of the wheel tread, thereby accelerating the calculation. Based on the Hertzian contact theory [15], the rail profile is divided longitudinally into a certain number of stripes. The wheel-rail penetration depth perpendicular to the rail head, as well as the local longitudinal and lateral curvatures, were calculated for each strip. These values were then weighted to determine the reference point and were used to obtain the contact patches and corresponding distribution. The normal damping forces were also taken into account to avoid high-frequency oscillation effects in wheel-rail contact calculation. Subsequently, the total normal force was obtained by summing the discrete normal contact forces and the normal damping forces within each strip of the contact patch. Using the Fastsim algorithm [16], the creepage, the creep reference velocity and the contact stress were calculated for each discrete strip. Based on the obtained normal force, contact patches and the friction coefficients, the total tangential forces can be statistically determined. Finally, the vertical and horizontal components of the total normal and tangential forces are calculated separately through coordinate transform. The resultant dynamic wheel-rail interactions such as the vertical wheel force can be obtained. In the wheel-rail contact calculation, the contact reference damping is set to 100000 Ns/m and the friction coefficient is taken as 0.4.

2.2 The turnout model

The high-speed turnout model was built by taking the No.18 turnout commonly used in China high-speed railway as a prototype. Turnout is a complex structure that has numerous components, especially rails with varying cross-sections along the track. The Bézier curve is used for rail cross-section fitting along the longitudinal direction to ensure a smooth transition of abovementioned rails. Each rail was built by using the Timoshenko beam element and the corresponding nodes were selected at intervals of every half span, i.e., approximately 0.3 m, via the finite element platform ABAQUS. The baseplate was also arranged according to the beam element configuration.

In the vertical direction, the bottom of rail is in contact with the baseplate through a layer of rubber tie plate, while the bottom of baseplate is in contact with the ground through another one. In the switch panel or the crossing panel, there are two or more rails contacting the same baseplate through a rubber tie plate. All the rubber tie plate were simulated using the spring-damping system. In the conversion area, the switch

machine is capable of converting and locking both the switch rail and the long point rail. The abovementioned rails directly contact the slide plate to ensure a smooth conversion process. Therefore, the spring-damping system with greater stiffness is used instead of the support of slide plate.

In the lateral direction, rails are constrained by the fastening system, also simulated by the spring-damping system. The iron blocks between the switch rail and the stock rail, and those between the long point rail and the wing rail, were modeled by the springs arranged horizontally along the track. In addition, the fillers between the wing rail and the point rail were modeled by springs with greater stiffness in six directions. There is a close fit between the straight switch rail and the curved stock rail, as well as between the long point rail and the wing rail when the turnout allows the train to pass in the through route. Therefore, springs along the lateral direction of the track are also used to simulate the corresponding fitting force.

Assuming that no special track disease including the longitudinal crawling of track and rail overturning, only four degrees of freedom were considered, i.e., sway, surge, pitch and yaw. As for the baseplate, heave and roll were considered.

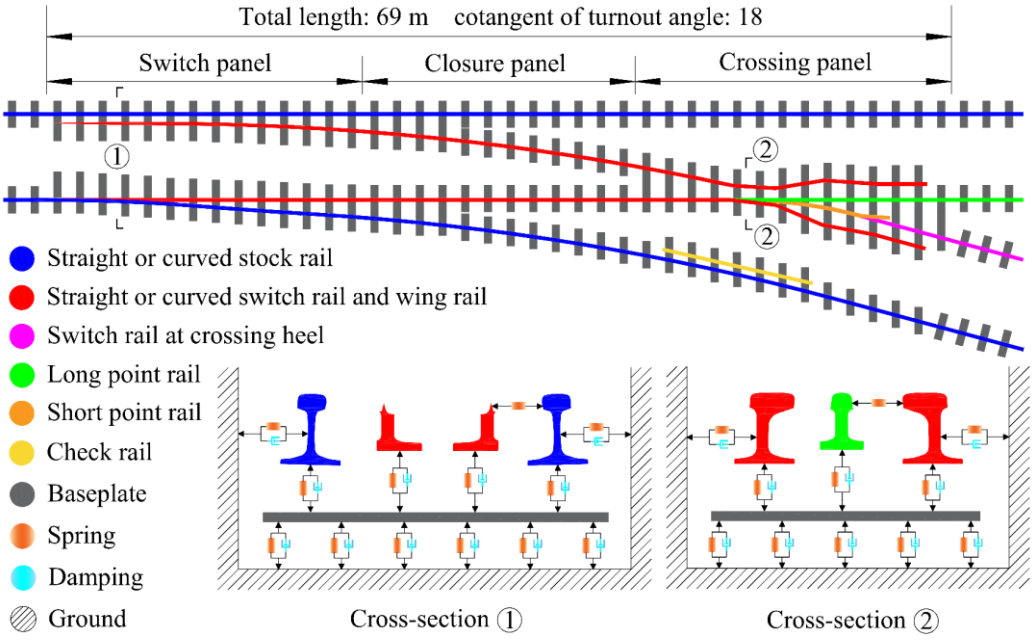

Figure 3: The simplified topology of the turnout model.

The master nodes of the substructure of the traditional track finite element model are still in a large number after the Craig-Bampton reduction [17], laying a heavy burden on computation. On the contrary, the modal superposition method [18] decouples the original dynamic equations and superimposes the modal contribution at different eigenfrequencies to obtain the overall deformation and free oscillation of the vehicle-turnout system. This method reduces the large number of degrees of freedom

of the original structure and greatly improves the computational efficiency. Assume that there is a system with multiple degrees of freedom as follows:

$$M\ddot{z} + C\dot{z} + Kz = P \tag{1}$$

where M represents the mass matrix, C represents the damping matrix, K represents the stiffness matrix, P represents the load matrix, z represents the nodal displacement matrix, respectively. Then, the free vibration of the system can be obtained as follows:

$$\left(K - \omega_a^2 M\right)\phi_a = 0, a = 1,2,3,...,n \tag{2}$$

where ω_a represents the natural frequency of the a^{th} -order vibration mode ϕ_a . Superimpose vibration modes and loads at all eigenfrequencies, respectively:

$$\mathrm{z} = \sum_{a=1}^{n} \phi_a u_a, a = 1,2,3,...,n \tag{3}$$

$$P = \sum_{a=1}^{n} \phi_a f_a, a = 1,2,3,...,n \tag{4}$$

where u_a represents the a^{th} -order vibration mode coordinate, f_a represents the a^{th} -order load, respectively. Different vibration modes are orthogonal to the generalized mass matrix and generalized stiffness matrix, respectively:

$$\phi_a^T M \phi_b = 0, a \neq b \tag{5}$$

$$\phi_a^T K \phi_b = 0, a \neq b \tag{6}$$

Thus, equation (1) can be rewrite as follows:

$$M_a \ddot{u}_a + C_a \dot{u}_a + K_a u_a = f_a, a = 1,2,3,...,n \tag{7}$$

where M_a represents the generalized mass matrix, C_a represents the generalized damping matrix, K_a represents the generalized stiffness matrix, respectively. Now introduce the following equation:

$$\lambda_a = \frac{C_a}{2\omega_a M_a}, a = 1,2,3,...,n \tag{8}$$

where λ_a is defined as the modal damping ratio. Thus, the dynamic equation of the system can be reshaped as follows:

$$\ddot{u}_a + 2\lambda_a \omega_a \dot{u}_a + \omega_a^2 u_a = \frac{f_a}{M_a}, a = 1,2,3,...,n \tag{9}$$

Then, the free vibration of the system can be obtained with certain modal damping ratios. To accurately simulate the high-frequency vibration of wheel and rail as well as the pinned-pinned bending resonance [19] and to achieve a balanced computational efficiency, the cut-off frequency and sampling frequency are both set at 2000 Hz in the turnout finite element model. As for the No. 18 high-speed turnout, the relevant relationship between modal damping ratio and natural frequency has not been determined and calibrated. The modal damping ration is taken as 0.02 with referring to reference [18].

2.3 Verification

This paper compared the simulation results with the field data for verification of the built coupled vehicle-turnout model. The field data was measured and obtained from the instrumented wheelset of the high-speed comprehensive inspection train. The instrumented wheelset is equipped with multiple sensors and high-precision measurement installations that can perform the real-time measurement, playback, calibration of the raw wheel-rail contact data. The simulation conditions kept consistency with actual measurement, such as the installation of the turnout, the turnout type, vehicle passing direction, speed, etc. Taking the vertical wheel force as an illustration for verification, the comparison between simulation result and field data is shown in Figure 4.

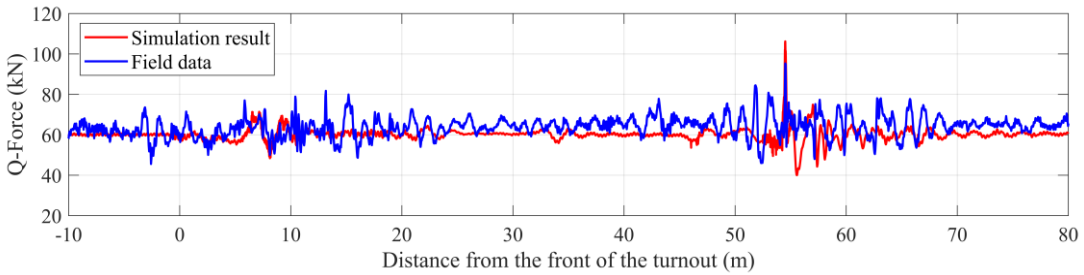

Figure 4: The comparison between simulation result and field data.

The field data is influenced by objective factors such as stochastic track geometric irregularities, polygonal wheel wear, rail wear, etc. As a result, there is a small difference between the field data and the ideal simulation result. In general, the comparison shows that the discrepancy is within the acceptable level. Vertical wheel force of both field data and simulation exhibits similar and significant fluctuations induced by the structural irregularities in the switch panel (mileage from 0 to 21 m) and the crossing panel (mileage from 46 to 69 m). In the closure panel (mileage from 21 to 46 m), both fluctuations decrease slightly. The maximum vertical wheel force of simulation result in the switch panel and the crossing panel is 71 kN and 106 kN, respectively, compared to 77 kN and 95 kN of the field data. Thus, the coupled vehicle-turnout model built in this paper can be acceptable for conducting relevant research on impact the stochasticity of inside distance between the wheelset has on the dynamic wheel-rail interactions.

3 The generalized density evolution equation

3.1 The stochastic distribution field

The traditional sampling method such as the Latin hypercube design, stratified sampling, Halton sequence and Hammersley sampling can be adopted to construct a stochastic distribution field for an input variable such as the inside distance between the wheelset. In this paper, the number theoretical method [20] was used for stochastic distribution field construction:

$$x_{j,m} = \frac{2mh_j - 1}{2n} - \mathrm{int}\left(\frac{2mh_j - 1}{2n}\right),\ j = 1,2,3,...,s;\ m = 1,2,3,...,n \tag{10}$$

where m represents the dimension of stochastic distribution field, h_j represents the integer operator, n represents the number of representative points, $\mathrm{int}(X)$ is used for retain the integer part of X, respectively. For a one-dimensional issue, h_1 is usually taken as 1. The points obtained from formula (10) are uniformly distributed within a unit hypercube. The corresponding joint PDF exhibits a spherically symmetric distribution. The further away the points are from the center of the hypercube, the smaller the PDFs are. In order to eliminate the points scattered in the corner of the hypercube whose contribution and influence to the stochastic distribution field are relatively small, the representative points can be screened by the following formula:

$$\sum_{j=1}^{s}\left[2\left(x_{j,m} - \frac{1}{2}\right)\right]^2 \le r^2,\ j = 1,2,3,...,s;\ m = 1,2,3,...,n \tag{11}$$

where r represents the bounded radius. When r equals to 1, the points scattered in the unit hyperball that are externally tangent to the unit hypercube are retained, while the others are omitted. Then, the samples of the actual stochastic filed can be constructed by the affine transformation:

$$K_{j,m} = 2(x_{j,m} - 0.5)\lambda,\ j = 1,2,3,...s;\ m = 1,2,3,...,n \tag{12}$$

where λ represents the border of the actual stochastic field. The assigned probability can be determined as follows:

$$P_m = p(K_{1,m}, K_{2,m}, K_{3,m}, ..., K_{j,m})V_m,\ j = 1,2,3,...,s;\ m = 1,2,3,...,n \tag{13}$$

$$V_m = \frac{(2\lambda)^2}{n},\ m = 1,2,3,...,n \tag{14}$$

where $p(K_{1,m}, K_{2,m}, K_{3,m}, ..., K_{j,m})$ represents the joint PDF of the samples.

By referring to the actual distribution of the gap between the wheel flange and the rail, this paper took the commonly used 1353 mm as the mean of the inside distance between the wheelset and a fluctuation of plus-minus 3 mm. Thus, the stochastic field of the inside distance between the wheelset distributed from 1350 mm to 1356 mm

was built. Given that the number of samples corresponding to a one-dimensional issue reaching 60 is sufficient [21], this paper selected 100 samples without loss of generality.

3.2 The finite difference method

The dynamic wheel-rail interactions of all samples were determined by the coupled vehicle-turnout model. The GDEE was used to describe corresponding evolutionary probabilistic characteristic over time:

$$\frac{\partial p_{X\Theta}\left(x,\theta,t\right)}{\partial t}+\dot{X}\left(\theta,t\right)\frac{\partial p_{X\Theta}\left(x,\theta,t\right)}{\partial x}=0 \tag{15}$$

where $p_{X\Theta}\left(x,\theta,t\right)$ represents the joint PDF of the probability-preserved field $\left(X,\Theta\right)$, $\dot{X}\left(\theta,t\right)$ represents the evolution speed of response, respectively. The initial PDF can be determined as follows:

$$p_{X\Theta}\left(x,\theta,t\right)=\delta\left(x-x_0\right)P_m \tag{16}$$

where x_0 represents the response at initial time, δ represents the operator of the Dirac function [22]. The GDEE is essentially a partial differential equation that can not be directly solved. A finite difference method, named the Lax-Wendroff scheme of the two-sided difference, can be adopted to solve such equations. However, the resultant response could show obvious high-frequency oscillation and energy dissipation. Instead, the Total Variation Diminish scheme of the two-sided difference not only solves above problems, but also reaches a high accuracy in the calculation [19]. The Courant-Friedrichs-Lewy condition must be met to ensure the evolutionary stability:

$$\left|\lambda b\right|\le 1 \tag{17}$$

The PDF of the response over time can be determined as follows:

$$p\left(x,t\right)=\int_{\Omega_\theta}p\left(x,\theta,t\right) \tag{18}$$

3.3 Verification

This paper cited the content of Chapter 5 of the authors' published paper [23] as a verification of the PDEM. The authors' conducted a comparison between the PDEM and the Monte Carlo method (MCM). The mean and standard deviation in time domain, obtained by GDEE corresponding to 109 samples, coincide well with those obtained by the MCM corresponding to 2000 samples. The PDEM, using much less samples and computation time, reaches the same accuracy as the MCM. In addition, the PDEM is capable of describe the continuously distributed PDF of response over

time and space that cannot be achieved by the MCM, featuring unparalleled efficiency and universality.

4 Simulation and analysis

This chapter calculated and analysed the PDF of various dynamic responses of vehicle passing through the turnout in the facing direction of through route, including the lateral displacement of the first wheelset and vertical wheel force. Considering that the wheel-rail impact in the vertical direction is more pronounced than the one in the lateral direction, this paper only discussed the corresponding PDF in the vertical direction. The speed of the vehicle passing through the right-hand single turnout in the facing direction of through route was set at 400 km/h. The PDFs of all responses are plotted via the contour map with 1000 levels.

4.1 The lateral displacement of wheelset

The positive and negative signs of the lateral displacement of the wheelset represents the directions towards the side of the straight stock rail and that of the straight switch rail, respectively. As the vehicle passes through the turnout, the curved stock rail gradually shifts outward and the wheel-rail contact point moves away from the wheel flange. The wheelset resultantly shifts towards the side of the straight stock rail and the difference of rolling radius of the wheel-rail contact point between the left and right wheel gradually increases. A distribution range from -0.8 mm to 1.4 mm was induced by the varying inside distance between the wheelset. A distinct bright red spot centred at approximately 15 m from the front of the turnout was captured. This indicates that the lateral displacement of wheelset shows clustering effect at this location after the wheel load transition, i.e., 1 mm, regardless of the varying inside distance between the wheelset. In the closure panel, the narrow evolutionary strip widens and the dark blue spot emerges. The corresponding PDF shows a significantly enhanced diffusivity with a distribution width reaching approximately 1.5 mm. In the crossing panel, the evolutionary strip tends to narrow again and then spread during the wheel load transition.

With the increase of the inside distance between the wheelset, as shown in Figure 5 (b), the wheelset deflects faster towards the side of straight stock rail before reaching 15 m from the front of the turnout. Afterwards, the wheelset reverses the direction of deflection towards the side of the straight switch rail. Therefore, a large inside distance between the wheelset is more likely to cause the vehicle to sway when the vehicle passes through a turnout, while also facilitating a faster alignment of the vehicle with the center of the track line.

4.2 The vertical wheel force

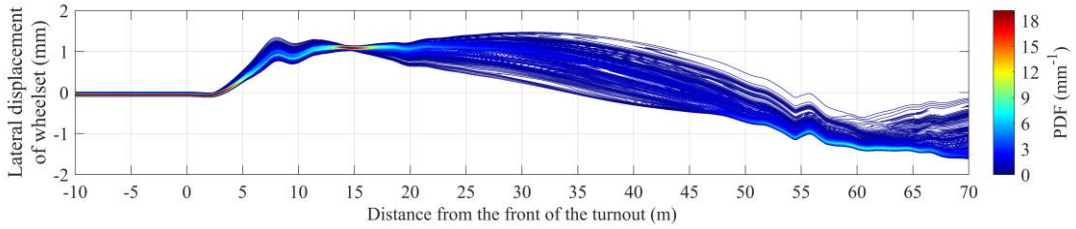

(a)

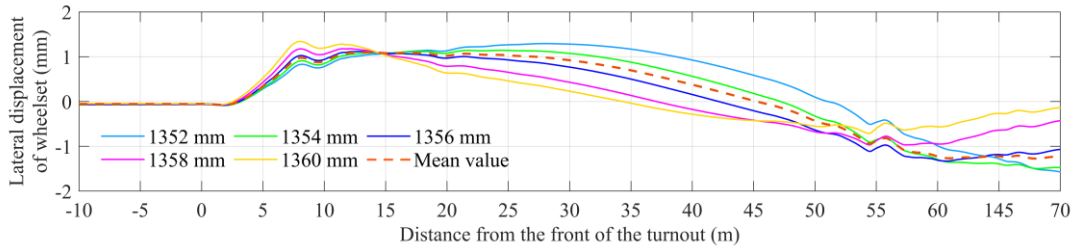

(b)

Figure 5: The lateral displacement of wheelset (a) The contour map of PDF (b) Comparison of results under various inside distances between the wheelset

Compared to the lateral displacement of the wheelset, the concentration of the vertical wheel force is stronger. As for the vertical wheel force on the straight stock rail, the distribution width of the evolutionary strip induced by the varying inside distance between the wheelset reaches only around 5 kN and there is basically no obvious change in the brightness and the spot colour. As the right wheel transfers from the curved stock rail to the straight switch rail, the vertical wheel force on the straight switch rail (mileage from 6 m to 12 m) exhibits a certain degree of diffusion, including a reduction in the red of the central region and an intensification of the blue at the edges. The corresponding of range on this side also exhibits around 5 kN. Similarly, in the crossing panel (mileage from 53 m to 54.3 m), the vertical wheel force becomes discrete from its previous highly concentration as the straight wing rail gradually derivates outward. This indicates that the variation of the inside distance between the wheelset, combined with the structural track geometric irregularities in both the switch panel and the crossing panel, can exacerbate the stochasticity of the vertical wheel force. In other regions, such as the closure panel and the one where the long point rail is located, the vertical wheel force remains relatively concentrated with a distribution range of around 5kN.

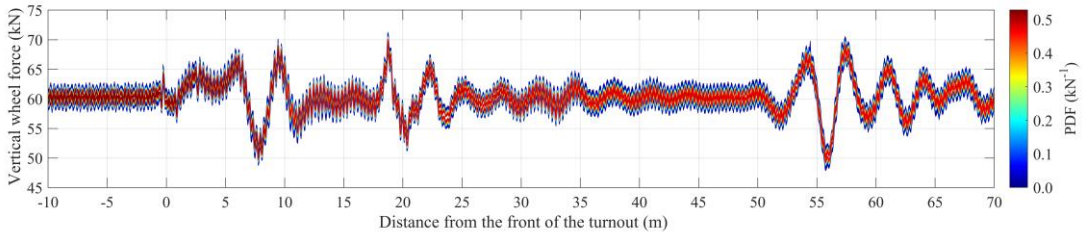

(a)

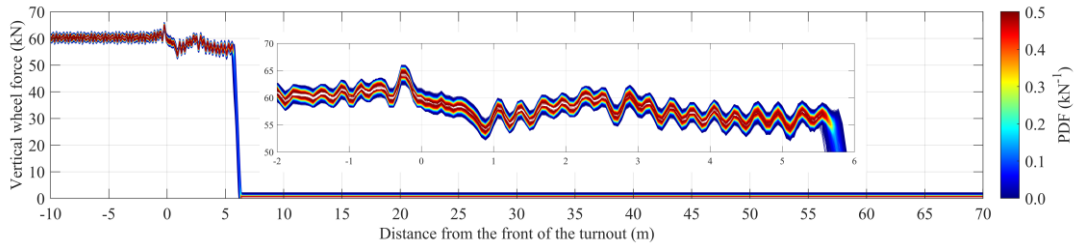

(b)

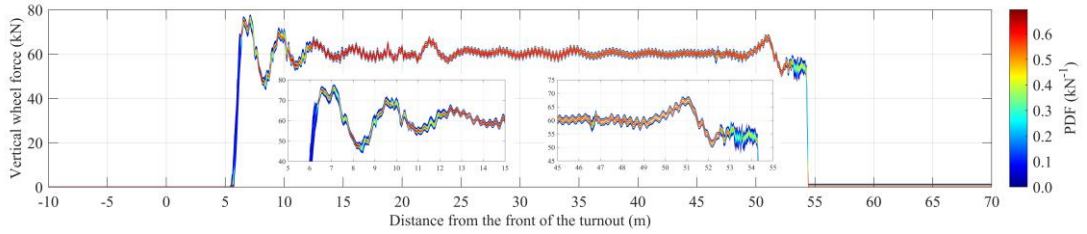

(c)

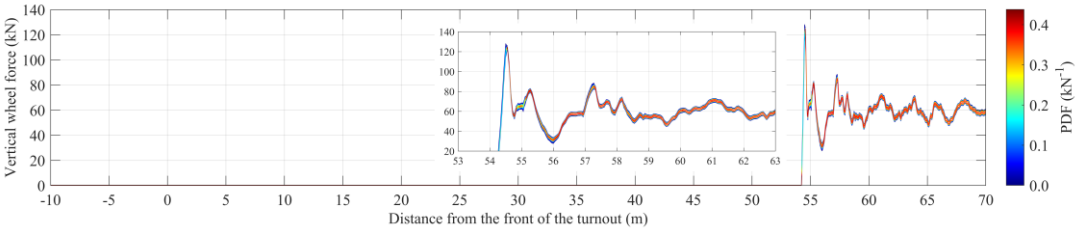

(d)

Figure 6: The vertical wheel force (a) On the straight stock rail side (b) On the curved stock rail side (c) On the straight switch rail and straight wing rail side (d) On the long point rail side

4.3 The wheel load transition

More importantly, the varying inside distance between the wheelset can also have a significant impact on the wheel load transition in both the switch panel and the crossing panel. This can be reflected from the alternating changes of vertical wheel forces on different rail sides, as shown in Figure 7. The mean curve was calculated by the superposition of the response mesh and corresponding PDFs obtained by the GDEE, whose reliability was validated in Section 3.3.

The declining process of vertical wheel force on the curved stock rail gradually shifts forward with increase of the inside distance between the wheelset in the switch panel. Specifically, the vertical wheel force completely decreases to 0 kN at around

6.39 m when the inside distance between the wheelset is 1350 mm. By increasing it to 1360 mm, the location at which the vertical wheel force completely decreases moves to around 6.15 m. The disappearance of the vertical wheel force on the curved stock rail during the wheel load transition is advanced by a distance of around 240 mm. Similarly, the starting location of vertical wheel force increase shifts from approximately 5.71 m to approximately 5.46 m when the inside distance between the wheelset increases from 1350 mm to 1360 mm. The appearance of the vertical wheel force on the straight switch rail is also advanced by a distance around 250 mm.

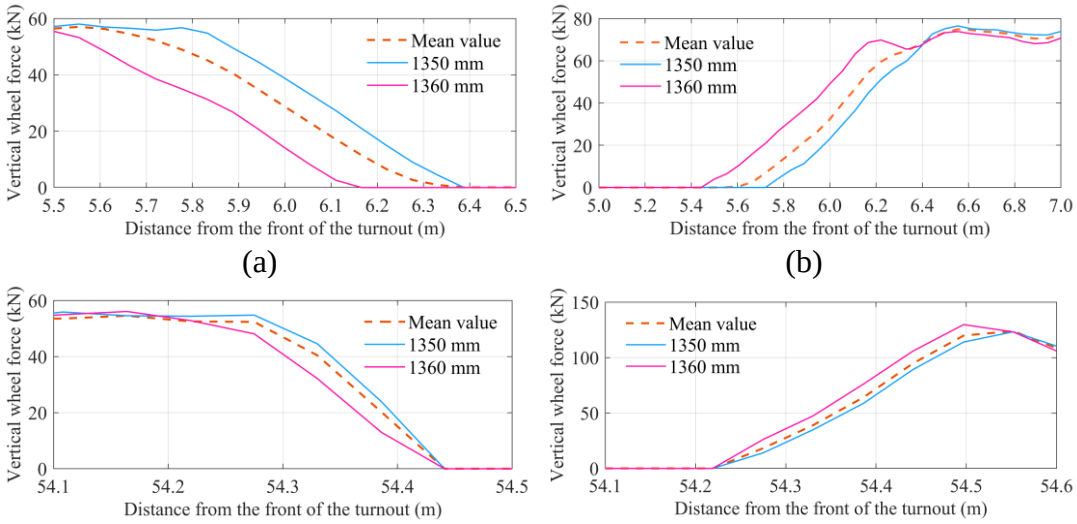

Figure 7: The vertical wheel force in the wheel load transition (a) On the curved stock rail (b) On the straight stock rail (c) On the straight switch rail (d) On the long point rail

While in the crossing panel, the situation is a little different. At the same location during the wheel load transition, the vertical wheel force on the straight wing rail is smaller when the inside distance between the wheelset is larger shown in Figure 7 (a) and (b), while the condition is quite the opposite of the corresponding change in the crossing panel shown in Figure 7 (c) and (d). This indicates that the varying inside distance between the wheelset does indeed affect the speed of change in the vertical wheel force. However, the location where the vertical wheel force on the straight wing rail completely decreases to 0 kN, as well as the one where the vertical wheel force on the long point rail begins to increase, remain unchanged when changing the inside distance between the wheelset. Thus, except for the speed of change in the vertical wheel force, the stochasticity of the inside distance between the wheelset has almost no impact on the wheel load transition.

4 Conclusions

Based on the number theoretical method, a stochastic distribution field of the inside distance between the wheelset is built. Within this field, A coupled vehicle-turnout model, with rail flexibility considered via the finite element analysis platform, was established by the modal superposition method. The PDFs of response of the vehicle

passing through a turnout in the facing direction of through route at a speed of 400 km/h, such as the lateral displacement of the wheelset and the vertical wheel force, were determined by the GDEE with TVD scheme. Some conclusions are drawn as follows:

1. The lateral displacement of wheelset in the closure panel exhibits a significant diffusion, while a relatively concentrated condition occurs near the wheel load transition in both the switch panel and the crossing panel. The lateral displacement of wheelset can be found around 1mm at around 15 m from the front of the turnout regardless of the varying inside distance between the wheelset.
2. The change of inside distance between the wheelset in the range from 1350 mm to 1360 mm can induce a distribution range of 5 kN of the vertical wheel force. The structural track geometric irregularities in both the switch panel and the crossing panel will intensify the influence of the inside distance between the wheelset on the stochasticity of the vertical wheel force in the wheel load transition.
3. In the switch panel, the location where the vertical wheel force on the curved stock rail completely decreases to 0 kN, and the one where the vertical wheel force on the straight switch rail starts to increase, are both advanced approximately by 240 mm to 250 mm when the inside distance between the wheelset increase from 1350 mm to 1360 mm. In the crossing panel, both the starting location and ending location of the wheel load transition are almost unaffected by the varying inside distance between the wheelset, except for the change of speed in the vertical wheel force.

Acknowledgements

The authors would like thank the support of the National Natural Science Foundation of China (52122810, 52108418, 52278464) and the Sichuan Science and Technology Program (2023NSFSC0884).

References

[1] H. C. Chen, T. Z. Huang, Q. W. Wang, et al. Test study on the influence of the distance between backs of the wheel flanges on rolling stock's dynamic performance, China Railway Science, 27(2006) 99-103.

[2] H. C. Chen, Q. W. Wang, T. Z. Huang, et al. Research on the selection of the distance between backs of the wheel flanges of the passenger traffic only line, Railway Locomotive & Car, 28(2008) 4-8.

[3] G. W. Xiao, X. B. Xiao, Z. F. Wen, et al. Comparison of Dynamic Behaviors of Wheelsets of High-speed Passenger Car, Journal of the China Railway Society, 30(2008) 29-35.

[4] R. Chen, Y. Ding, J. Y. Chen, et al. Influence of different wheel tread on static wheel-rail contact behavior in subway turnout area, Journal of Central South University (Science and Technology), 51(2020) 2624-2633.

[5] N. Wu, J. Zeng. Investigation into wheel-rail contact geometry relationship and wheel wear fatigue of high-speed vehicle, China Railway Science, 35(2014) 80-87.

[6] C. G. Wang, Y. F. Wang, H. T. Li, et al. Comparative analysis on high-speed wheel/rail contact geometric, Railway Locomotive & Car, 26(2006) 1-5.

[7] R. Luo, J. Zeng, P. B. Wu, et al. Influence of wheel/rail parameters on wheel profile wear of high-speed train, Journal of Traffic and Transportation Engineering, 9(2009) 47-63.
[8] Y. Y. Qi, H. Y. Dai, C. Y. Song, et al. Shaking analysis of high-speed train's carbody when cross lines, Journal of Mechanical Science and Technology, 3(2019) 1055-1064.
[9] H. L. Shi, J. Y. Guo, Y. Wang, et al. Dynamic performance of high-speed gauge-changeable railway vehicle, Journal of Mechanical Engineering, 56(2020) 98-105.
[10] Q. S. Zhang, Q. B. Zhai, J. M. Ding, et al. An Efficient Method for Dynamic Measurement of Wheelset Geometric Parameters, IEEE Transactions on Instrumentation and Measurement, 72(2023).
[11] L. H. Fang, Q. H. Guan, Z. F. Wen. Influence of wheelset bending on wheel-rail contact of vehicles with inside and outside axle boxes, Journal of Central South University (Science and Technology), 53(2022) 3259-3269.
[12] T. D. Hien, M. Kleiber. Stochastic structural design sensitivity of static response, Computers & Structures, 38(1991) 659-667.
[13] N. Wiener. The homogeneous chaos, The johns Hopkins University Press, 2012.
[14] J. Li, J. B. Chen, W. L. Sun, et al. Advances of the probability density evolution method for nonlinear stochastic systems, Probabilistic Engineering Mechanics, 28(2012) 132-142.
[15] Michel Sebès, Luc Chevalier, Jean-Bernard Ayasse. A fast-simplified wheel–rail contact model consistent with perfect plastic materials, Vehicle System Dynamics, 50(2012) 1453-1471.
[16] J. J. Kalker. A Fast Algorithm for the Simplified Theory of Rolling Contact, 11(1982) 1-13.
[17] Roy R. Carig Jr, Mervyn C. C. Bampton. Coupling of Substructures for Dynamic Analyses, AIAA Journal, 6(1968) 1313-1319.
[18] B. A. Pålsson, R Ambur, M Sebès, et al. A comparison of track model formulations for simulation of dynamic vehicle–track interaction in switches and crossings, Vehicle System Dynamics, (2021).
[19] W. M. Zhai. Vehicle-track coupled dynamics theory and applications, Science Press & Springer, 2020.
[20] J. Li, J. B. Chen. The number theoretical method in response analysis of nonlinear stochastic structures, Computational Mechanics, 39(2007) 693-708.
[21] J. B. Chen, J. Li. Strategy of selection points via number theoretical method in probability density evolution analysis of stochastic response of structures, Chinese Journal of Theoretical and Applied Mechanics, 38(2006) 134-140.
[22] J. Li, J.-b. Chen, Stochastic dynamics of structures, John Wiley & Sons (Asia) Pte Ltd, 2009.
[23] Z. Yan, S. X. Li, J. M. Xu, et al. Random analysis of dynamic wheel–rail interactions in the switch panel of a turnout with geometric tolerances based on the probability density evolution method, Vehicle System Dynamics, (2022).